PNAS RESEARCH ARTICLE | BIOPHYSICS AND COMPUTATIONAL BIOLOGY
EVOLUTION OPEN ACCESS

Passive endocytosis in model protocells

Stephanie J. Zhang[a,b,1], Lauren A. Lowe[c,d,e], Palapuravan Anees[f,g], Yamuna Krishnan[f,g,h], Thomas G. Fai[i,2], Jack W. Szostak[a,b,g,j,2], and Anna Wang[c,d,e,2]

Edited by Gerald Joyce, Salk Institute for Biological Studies, La Jolla, CA; received January 2, 2023; accepted May 10, 2023

Semipermeable membranes are a key feature of all living organisms. While specialized membrane transporters in cells can import otherwise impermeable nutrients, the earliest cells would have lacked a mechanism to import nutrients rapidly under nutrient-rich circumstances. Using both experiments and simulations, we find that a process akin to passive endocytosis can be recreated in model primitive cells. Molecules that are too impermeable to be absorbed can be taken up in a matter of seconds in an endocytic vesicle. The internalized cargo can then be slowly released over hours, into the main lumen or putative cytoplasm. This work demonstrates a way by which primitive life could have broken the symmetry of passive permeation prior to the evolution of protein transporters.

vesicles | membranes | lipids | origin of life | budding

Significance

In contemporary life, a molecule's permeability across cell membranes is tightly regulated by protein transporters. How did primitive cells obtain nutrients, prior to the advent of such transporters? Molecules can passively diffuse across membranes, but importing nutrients in this manner would require a primitive cell to reside in a pool of nutrients for hours if not days. If the membrane is too permeable, nutrients would leak out as soon as they enter. Worse still, leaky membranes would lose primordial genetic material. We present a physicochemical method for triggering passive endocytosis in model primitive cells. The import of nutrients into a stable internalized compartment enables the model primitive cell to gradually absorb the nutrients, thereby breaking the symmetry of passive permeation.

In extant life, membranes provide a selective barrier between a cell and its environment, which enables the inheritance of adaptive traits and ultimately leads to Darwinian evolution (1, 2). Life itself may have emerged from self-replicating informational molecules spatially constrained by primitive membranes (1–3). Among various lipid candidates, fatty acids are particularly well suited as the components of primitive membranes owing to their prebiotic relevance (4, 5) and dynamic exchange properties (6, 7). The possible involvement of fatty acid vesicles in the origin of life has been further demonstrated by their ability to grow and divide without complex biochemical machinery (8–10) and to encapsulate RNA templates that are being nonenzymatically copied (11, 12).

In nascent life, the absence of protein transporters implies that a protocell enveloped by lipid bilayers would have had to rely on passive diffusion for internalizing nutrients (13–15). Diffusive transport across the membrane is symmetric and is driven purely by the concentration gradient of solutes across the membrane. Despite this, the fluxes need not be the same. When the symmetry is broken, for example, by placing a nutrient sink within the cell, or by a changing external environment, there can be a net flux into or out of the protocell. However, under transient nutrient-rich circumstances, the low permeability of primitive membranes, needed to prevent the loss of the encapsulated cargo, also delays the efficient acquisition of nutrients. Hence, a protocell would have to reside within a pool of nutrients for hours to absorb useful levels of polar or charged molecules (12, 15). Whether physicochemical stimuli can fuel nondiffusive transport mechanisms remains an important question because such mechanisms could break the transmembrane symmetry in a way that could bias the inward nutrient flow, or expedite nutrient import.

One type of transport that has both "active" and "passive" modes is endocytosis. In modern biology, the inward budding of lipid membranes can be active such as in receptor-mediated endocytosis, or passive as in fluid-phase endocytosis. Such a higher-order topological transformation has been previously demonstrated in phospholipid membranes via various pathways (16–18). However, the ability of model primitive membranes to endocytose, i.e., internalize cargo from the external milieu, has yet to be definitively shown. Model primitive membranes typically consist of lipids with dynamic properties distinct from those of phospholipids and thus the routes to engender shape changes could potentially differ (19). For instance, flip-flop of model primitive membrane lipids rapidly relaxes any curvature stress (20) that might otherwise help drive the shape transformation and help overcome the energy barrier required for a topological change (19). On the contrary, flip-flop may also be useful for enabling the membrane to adopt the extreme configurations required for inward or outward budding.

Here, we demonstrate that primitive cell compartments composed of fatty acids can passively endocytose via a purely physicochemical process. A simultaneous reduction in volume and increase in surface area allows larger molecules to be imported via an inward bud into model protocells, mimicking the process of passive endocytosis in complex eukaryotes. This process takes only seconds, similar to modern forms of endocytosis. The

Author contributions: S.J.Z., L.A.L., T.G.F., J.W.S., and A.W. designed research; S.J.Z., L.A.L., T.G.F., and A.W. performed research; P.A., Y.K., T.G.F., and J.W.S. contributed new reagents/analytic tools; S.J.Z., L.A.L., T.G.F., J.W.S., and A.W. analyzed data; and S.J.Z., L.A.L., P.A., Y.K., T.G.F., J.W.S., and A.W. wrote the paper.

The authors declare no competing interest.

This article is a PNAS Direct Submission.

[1]Present address: Department of Pathology, Brigham and Women's Hospital, Harvard Medical School, Boston, MA 02115.

[2]To whom correspondence may be addressed. Email: tfai@brandeis.edu, jwszostak@uchicago.edu, or anna.wang@unsw.edu.au.

This article contains supporting information online at https://www.pnas.org/lookup/suppl/doi:10.1073/pnas.2221064120/-/DCSupplemental.

Published June 5, 2023.

protocells continue to retain the internalized solutes even when removed from the nutrient source, and are thereby provided time to absorb the nutrients. Further, we construct a numerical model that captures such out-of-equilibrium shape changes. Taken together, we believe this marks an important step toward understanding the development of solute internalization and transport in primitive cells.

Results and Discussions

Fatty Acid Vesicles Undergo Membrane Invagination and Internal Budding. Here, we study the shape transformations and subsequent topological transitions of fatty acid vesicles in response to volume and area perturbations. For a sphere to change shape, it must have an increase in surface area-to-volume ratio. In principle, this can be accomplished via two pathways: by reducing the volume or increasing the surface area. We explore shape changes obtained through combinations of these pathways. We use hyperosmotic shocks to draw water out of the vesicles and reduce the internal volume; the magnitude of the osmotic shock is denoted as a change in concentration of the salt (Na-bicine), ΔC_V, from its starting point of 50 mM. We achieve membrane area growth by adding alkaline oleate micelles to a buffered solution of vesicles; the increase in total membrane lipid is denoted as a change in lipid concentration, ΔC_A, relative to a starting lipid concentration of 0.5 mM. Evaluations of the vesicle radius before and after micelle addition suggest that the increase in surface area is no more than twofold under the conditions used in this work (*SI Appendix*). To observe shape changes in real time with fluorescence microscopy, we prepared oleic acid/oleate (C18:1) giant unilamellar vesicles (GUVs) encapsulating water-soluble and membrane-impermeable fluorescent dyes (either 0.5 mM HPTS 8-hydroxypyrene-1,3,6-trisulfonic acid trisodium salt, or 1 mM calcein blue). These vesicles were then diluted tenfold into buffer that was identical in composition and pH to the original buffer (but lacked the lipids and dyes) to provide good contrast between encapsulated and unencapsulated dyes, enabling visualization of the dye encapsulated within vesicles.

We previously reported that an increase in lipid concentration by micelle addition (ΔC_A = 1 mM) to oleate GUVs results in outward budding, with the GUVs transforming into a series of smaller vesicles in close proximity, and possibly still connected by tethers (Fig. 1*A*) (9). Addition of a higher concentration of micelles (ΔC_A > 1 mM) resulted in vesicle division. In terms of a putative geological setting for such an event, fluid flow from precipitation, in pools, or from tectonic or volcanic events that drive hydrothermal processes, might have carried and mixed nutrients, mineral particulates, and lipid components. Such episodic events

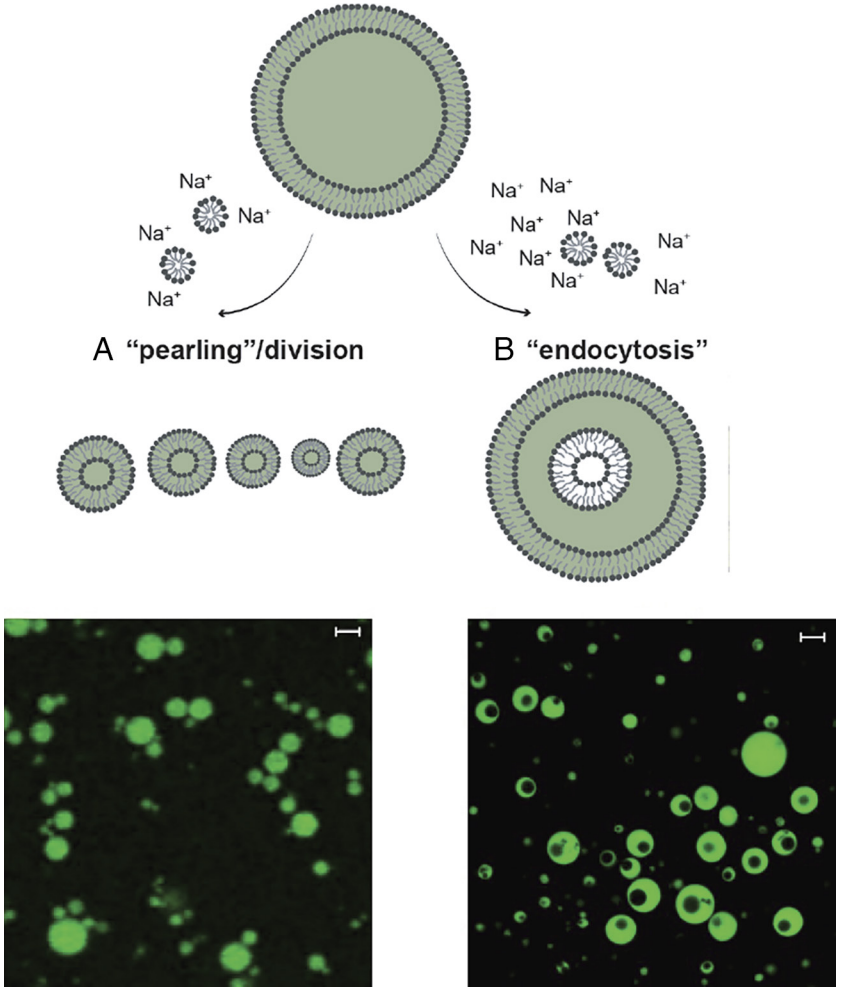

Fig. 1. Schematics and confocal micrographs of topological transformations of oleic acid/oleate GUVs following addition of oleate micelles or exposure to hyperosmotic shock. (*A*) Outward budding of GUVs was induced by micelle addition (stimulus B; ΔC_A = 1 mM). The resulting smaller, closely spaced vesicles can be seen in the confocal micrographs. This is similar to the supplemental videos shown in our previous work (9). (*B*) GUVs could be induced to "endocytose" upon a hyperosmotic shock coupled with micelle addition (stimulus A; ΔC_V = 100 mM, ΔC_A = 1 mM. See also Movie S1). Confocal micrographs reveal that vesicles initially containing 0.05 M Na-bicine and labeled with 0.5 mM HPTS (green fluorescence) have compartments that appeared as dark voids. Scale bars represent 5 μm.

from fluid flow–induced geochemical processes might result in fluctuations in osmotic pressures and simultaneous release of nutrients and lipids. Because increasing the surface area and reducing the internal volume would be predicted to increase the surface area-to-volume ratio, we expected that doing both simultaneously, denoted as stimulus A (ΔC_V = 100 mM, ΔC_A = 1 mM), might also cause vesicle division.

Instead, a series of different dramatic shape transformations occurred upon a simultaneous introduction of membrane material and an osmotic shock (Fig. 1*B*, *SI Appendix*, Fig. S1, and Movies S1–S8; please see *Materials and Methods* for exact experimental conditions). Specifically, GUVs appeared to elongate, then rapidly transform first into a stomatocyte via invagination and then into a sphere. We confirmed that the topological transformation was to a vesicle-in-vesicle structure rather than a torus by taking sectional image slices along the z-axis and reconstructing the volume in 3D (Movie S2). Further, we performed two distinct experiments to show that the internal vesicles are indeed fully separated from the external membrane. First, we added an aqueous dye, Alexa 594 hydrazide, that is exclusively aqueous and does not bind to membranes, to a final concentration of 10 μM. Alexa 594 hydrazide stayed completely outside of the GUV and did not enter the interior of the endocytosed vesicles, which demonstrates that the inner vesicles are not connected to the outside (*SI Appendix*, Fig. S2). Second, we added the dye Voltair^{PM} (21) (final concentration: 250 nM) which localizes to the fatty acid membrane by its POPE (1-palmitoyl-2-oleoyl-sn-glycero-3-phosphoethanolamine) moiety, but cannot flip-flop across the external membrane or reach any inner compartment owing to its conjugation to polar DNA oligonucleotides. The observation that only the GUV outer membrane leaflet became labeled excludes the possibility that the inner vesicle membranes are connected to the outer GUV membrane (*SI Appendix*, Fig. S3). Therefore, we can conclude that instead of budding *outward* (stimulus B; ΔC_V = 0 mM, ΔC_A = 1 mM Fig. 1*B*), the vesicles had budded *inward*. We hypothesize that the complete budding of an internal vesicle was possible because both the generated lateral tension from the insertion of lipids into the outer leaflet and the curvature stress from flip-flop not transporting lipids into the inner leaflet as rapidly as lipids inserting into the outer leaflet were sufficient to overcome the energies required for breaking the neck and completing the budding process (22). The exact mechanism is still uncertain, and should be the subject of future work.

Protocells Take Up Cargo Passively Following Membrane Invagination. As previously mentioned, micelle addition by itself leads only to outward budding (8, 9). Interestingly, micelle addition (ΔC_A = 0.5 mM to 5 mM) accompanied by varying levels of osmotic shock (ΔC_V = 25 mM to 100 mM) consistently led to inward budding. By exploring this two-dimensional parameter space, we found that the efficiency of internal compartment formation increased with the magnitude of the surface area increase. As more micelles were added (ΔC_A = 0.5 mM to 5 mM), the fraction of vesicles with internal compartments increased, and this effect was evident across all magnitudes of osmotic shock (ΔC_V = 25 to 100 mM, Fig. 2. See also Table 1). For example, the population of vesicles with internal compartments increased from approximately 7.3 ± 1.3% (ΔC_A = 0.5 mM; ΔC_V = 100 mM, total vesicles analyzed = 3,840) to approximately 88.5 ± 3.0% (ΔC_A = 5 mM; ΔC_V = 100 mM, total vesicles analyzed = 1,169).

We also found that the number of internal compartments could be tuned by varying the magnitude of the osmotic shock. At concentrations of added micelles between 2.5 mM and 5 mM, increasing the osmotic shock increased both the number of vesicles with compartments and the occurrence of multicompartment vesicles. For example, at an added micelle concentration of 5 mM, the fraction of vesicles with internal compartments increased from approximately 70.1 ± 9.9% (at ΔC_V = 25 mM, total vesicles analyzed = 695) to approximately 88.5 ± 3.0% (at ΔC_V = 100 mM, total vesicles analyzed = 1,169), while the fraction of multicompartment vesicles increased threefold from approximately 12.3 ± 3.0% (ΔC_V = 25 mM, total vesicles analyzed = 695) to approximately 36.2 ± 8.7% (ΔC_V = 100 mM, total vesicles analyzed = 1,169).

Creating two- or multi-compartment vesicles required a higher concentration of added micelles for lower osmotic shocks: A non-negligible yield of two-compartment or multicompartment vesicles required ΔC_A = 5 mM at a lower osmotic shock (ΔC_V = 25 mM), whereas it required only ΔC_A = 2.5 mM at a higher osmotic shock

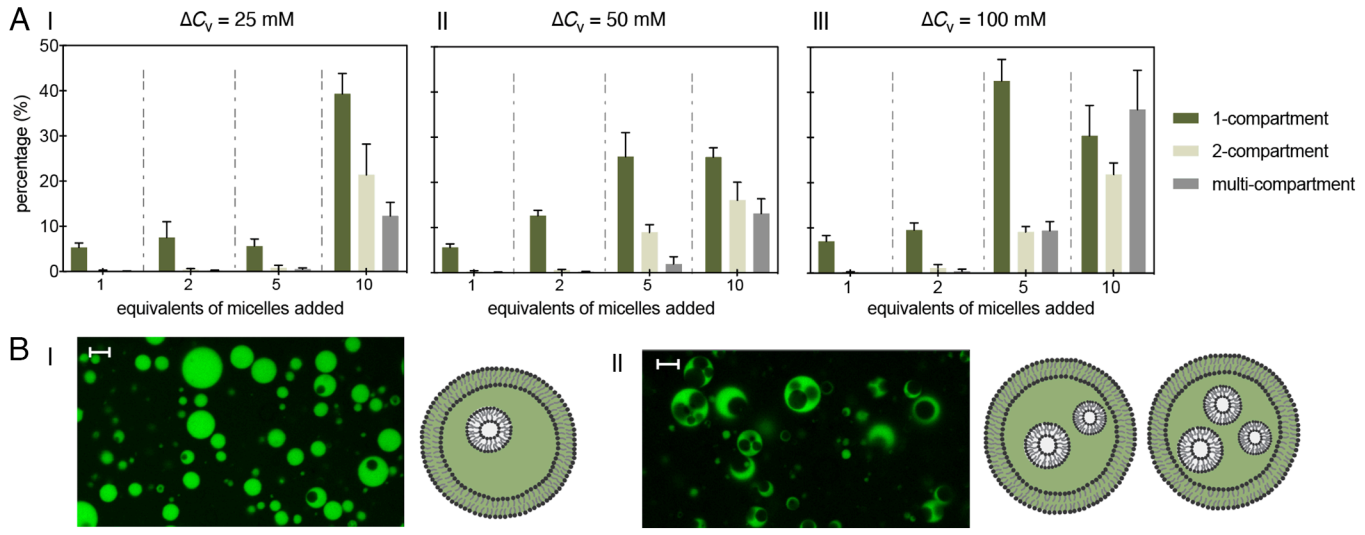

Fig. 2. Number of compartments per vesicle as a function of osmotic shock and micelle addition. Conditions are summarized in Table 1. (*A*) Distributions of compartments per vesicle for osmotic shocks and micelle additions of different magnitudes [ΔC_V = 25 (*i*), 50 (*ii*), 100 (*iii*) mM Na-bicine, ΔC_A = 0.5, 1, 2.5, 5 mM oleate]. The equivalents of oleate in the micellar solution added are defined with respect to the concentration of oleate/oleic acid in the starting vesicle suspension. (*B*) Representative confocal micrographs of vesicles with (*i*) single and (*ii*) multiple internal compartments. Scale bars represent 5 μm. Each condition consisted of at least five replicates, and error bars indicate the SD from the mean. The total number of analyzed vesicles for each condition is indicated in Table 1.

(ΔC_V = 100 mM). At lower concentrations of added micelles (ΔC_A = 0.5 mM to 1 mM), varying the magnitude of osmotic shock (ΔC_V = 25 mM to 100 mM) did not lead to significant changes in the number of internal compartments formed.

Having determined that the inward budding was robust, we then tested whether this pathway allowed for the passage of large polar molecules into protocells prior to the evolution of complex protein machinery. We found that passive endocytosis allowed the long DNA–dye conjugate (5′-Cy5-$C_{(10)}$ $A_{(18)}$-3′) (Fig. 3*A*) to be imported from the external medium into the vesicle itself. Specifically, the Cy5-labeled DNA 28-mers (appearing magenta) were introduced along with the simultaneous osmotic shock and micelle addition (stimulus A) into oleic acid/oleate GUVs containing encapsulated calcein blue (appearing blue). The resultant formation of magenta interior compartments indicates that the Cy5-labeled DNA 28-mers were successfully transported to the lumen of the internalized vesicles and thereby internalized by the GUVs (Fig. 3 *B*, *i* and *ii*).

The resultant vesicle-in-vesicle structures were not expected to preclude further inward budding events. We therefore tested whether repeated inward budding could be induced by successive rounds of simultaneous osmotic shock and micelle addition (stimulus A). Following the intake of Cy5-labeled DNA 28-mers into one set of internalized buds, a second simultaneous osmotic shock and micelle addition event was induced in the presence of the yellow aqueous compound fluorescein-12-UTP in the exterior solution. This resulted in the UTP being internalized via a second set of buds: The blue vesicles contained both magenta and yellow inner compartments (Fig. 3 *B*, *iii*). With both stimulus events being in the regime where two or more internal compartments are likely (Fig. 2), the resultant vesicles displayed a high internal volume fraction of internalized vesicles. The excess micelles introduced also led to de novo vesicle formation: Magenta vesicles containing yellow inner compartments are also occasionally observed. Some compartments also appear intermediate in color (e.g., orange), suggesting that some mixing between compartments might have occurred.

This result is informative for two reasons. First, the presence of inner compartments that are of a different color from the external medium (after two cycles of micelle addition in the presence of different dyes) indicates that the shape transformation of the vesicles does not end in the stage of stomatocytes (*SI Appendix*, Fig. S1*A*). Rather, inward vesiculation was completed and a full topological transformation had occurred (*SI Appendix*, Fig. S1*B*). Without the final topological transformation, all the endocytic compartments would be of the same color as the external medium. Second, the presence of both yellow and magenta internal compartments is consistent with two separate rounds of endocytosis having taken place. This confirms that the simultaneous osmotic shock and micelle addition event can trigger repeated endocytic events.

Release of Cargo from Internal Compartment into the Main Lumen. A substantial uptake of nutrients from the external solution by passive diffusion across the limiting membranes of protocells requires protocells to reside within the pool of

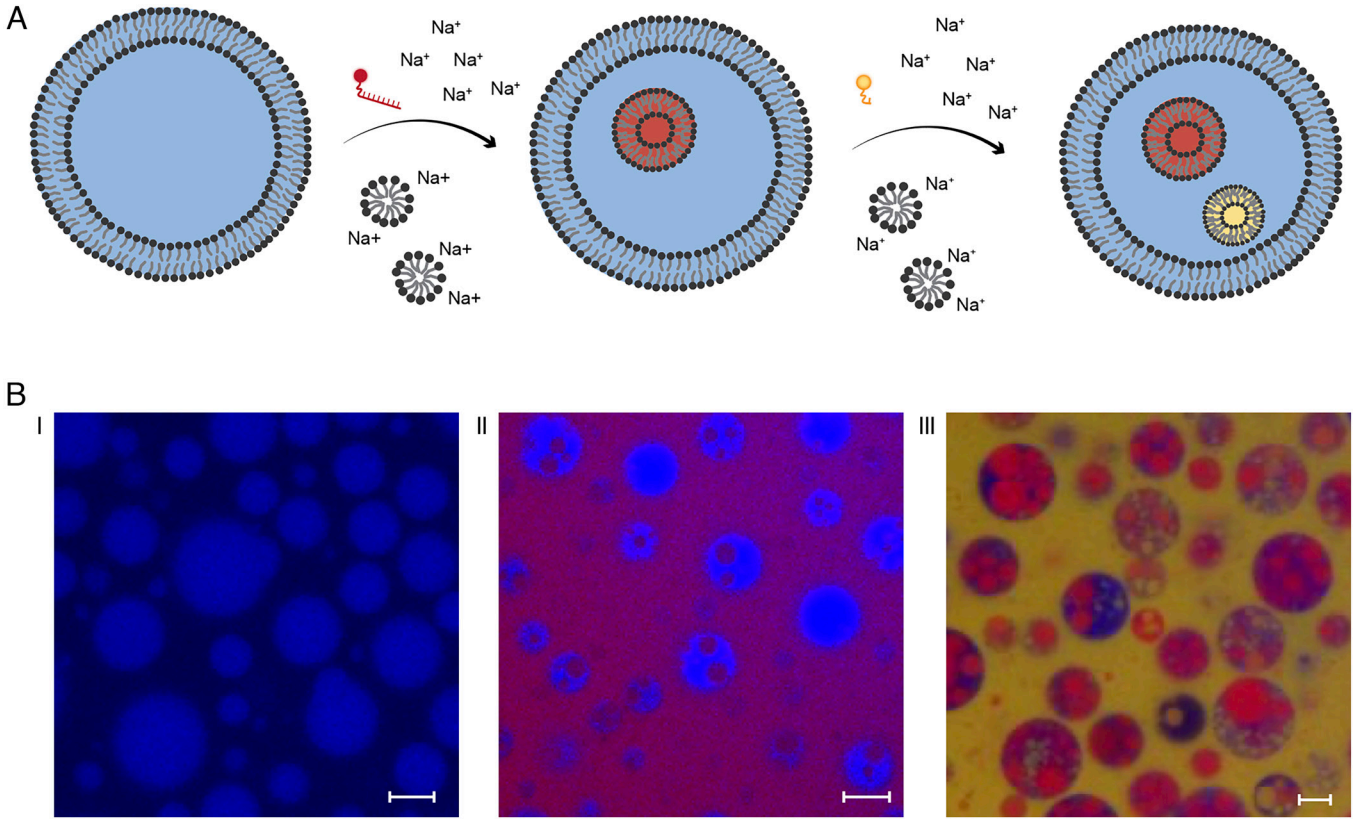

Fig. 3. Induction of multiple sequential passive endocytosis events. (*A*) Schematic for induction of multiple passive endocytosis events induced by successive osmotic shocks coupled with micelle additions. (*B*) Confocal micrographs of fatty acid vesicles with various numbers and sizes of interior compartments. (*i*) Initial GUVs with encapsulated calcein blue (blue). (*ii*) Simultaneous addition of 1 μM 5′-Cy5-$C_{(10)}$ $A_{(18)}$-3′, ΔC_V = 100 mM Na-bicine, and ΔC_A = 2.5 mM oleate resulted in inner compartments containing encapsulated 5′-Cy5-$C_{(10)}$ $A_{(18)}$-3′ (magenta) derived from the external solution. (*iii*) A second round of passive endocytosis stimulated by the simultaneous addition of 5 μM Fluorescein-12-UTP, ΔC_V = 100 mM Na-bicine, and ΔC_A = 2.5 mM oleate resulted in new inner compartments containing encapsulated Fluorescein-12-UTP (yellow) derived from the external solution. Scale bars represent 5 μm. The introduction of multiple heterogeneous stimuli to a uniform starting solution of vesicles ultimately leads to the emergence of population diversity (see also Movie S12).

nutrients for hours. By contrast, passive endocytosis results in a net inward flow of cargo within seconds, although the cargo is still contained within a membrane. Releasing nutrients stored inside the endocytic compartments into the main lumen, i.e., putative cytoplasm, would allow them to interact with other components within the protocell and is the final critical step in this pathway for nutrient uptake. For example, this could enable dinucleotides to interact with replicating internal oligonucleotides.

To test the ability of the internal endocytic compartment to release nutrients, we first used a relatively impermeable substrate, the fluorescein-labeled cyclic dinucleotide (cGAMPfluo), as a fluorescent tracer. cGAMPfluo was introduced along with a simultaneous osmotic shock and micelle addition (ΔC_V = 100 mM, ΔC_A = 1 mM) to oleic acid/oleate GUVs (Fig. 4*A*). The vesicles were then diluted fivefold into a 200 mM glucose buffer that was identical in composition and pH to the original buffer but lacked the lipids and cGAMPfluo, to dilute the free cGAMPfluo in the external medium. We then took confocal microscopy images over time to measure the fluorescence intensities in the internalized compartments, the main lumen of the GUVs, and the external medium. The fluorescence intensity serves as a measure of the relative concentrations of encapsulated material.

Tracking the fluorescence intensity of the internalized compartments relative to the external medium (Fig. 4*A*), which we consider an infinite bath, showed a decrease from 6.2 ± 1.0 to 3.9 ± 0.9 (N = 124) over 24 h. This suggests that the oligomer was slowly released by the internalized compartment, into the main lumen. Indeed, the fluorescence intensity of the internalized compartments relative to the main lumen decreased more than twofold, from the ratio of 36.3 ± 1.7 to 14.3 ± 1.1 over 24 h (Fig. 4*B*, N = 113). This indicates that the oligonucleotide was slowly released from the internalized compartment into the main lumen. We found similar results for another representative molecule with low permeability to fatty acid membranes (23), HPTS (*SI Appendix*, Fig. S5). Overall, these results demonstrate that internalized compartments can be used as nutrient storage depots, which would slowly release contents to the main lumen or "cytoplasm" of a protocell. Overall, our studies show that protocells are capable of a primitive form of endocytosis consisting of three characteristic steps: membrane invagination and budding, uptake of soluble external cargo into the resultant internalized compartments, and cargo release from the compartments into the main lumen. These constitute the three basic steps of all forms of modern endocytosis.

Modeling Out-of-Equilibrium Topological Changes. To understand the reason for invagination, we model the vesicle as an inextensible elastic material with prescribed bending modulus, spontaneous curvature, and permeability. While the model cannot predict whether a full topological transformation can occur, it does enable the prediction of morphological changes preceding a potential topological transition. The surrounding fluid is considered as an aqueous solution that contains amphiphiles that incorporate into the vesicle membrane at a given rate. As shown in the study by Ruiz-Herrero et al. (19), the resulting behavior may be described in terms of two dimensionless parameters that govern the steady-state vesicle morphology. In addition, to capture the effect of osmotic shocks, we include the possibility of osmotic pressures that drive flows across the membrane. This is done by adding an appropriate normal force to the membrane surface corresponding to the van't Hoff pressure $p = ck_BT$, where c is the difference in osmotic concentrations across the membrane.

After applying osmotic shocks in the presence of permeation and membrane growth, we observe that vesicles develop stomatocyte morphologies that progress spontaneously to develop inward buds (Fig. 5 *A* and *B*). The initial hyperosmotic shock causes the vesicles to shrink in volume while adding additional surface area. This increases the surface area-to-volume ratio over time. We use parameters listed in Table 2 and confirm that the timescales of

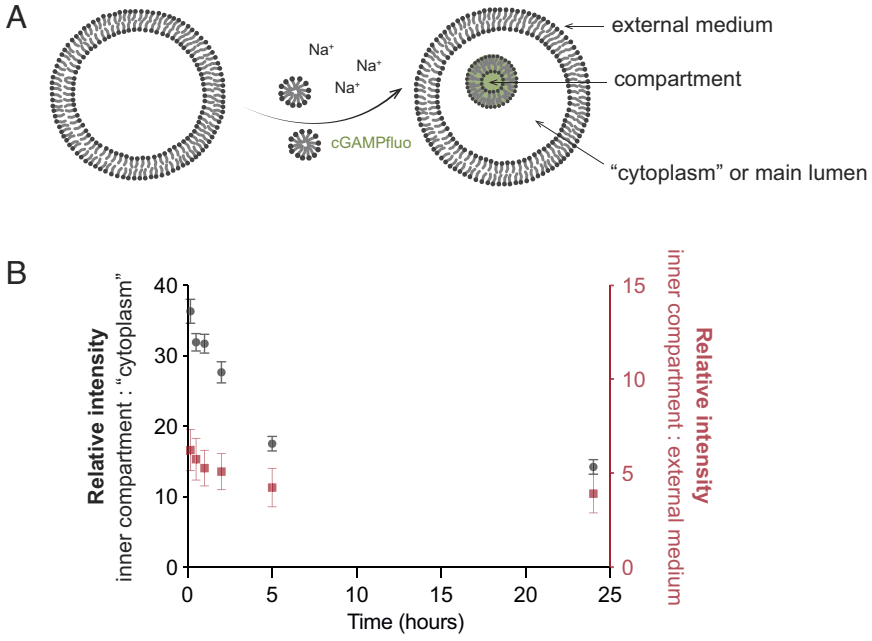

Fig. 4. Internal compartments can slowly deliver nutrients of low permeability to the main lumen or "cytoplasm" of a protocell. (*A*) Schematic of fluorescein-labeled cyclic dinucleotide (cGAMPfluo), a relatively impermeable substrate, being encapsulated in the interior compartment via one hyperosmotic shock coupled with micelle addition (ΔC_V = 100 mM Na-bicine, ΔC_A = 2.5 mM oleate, $C_{cGAMPfluo}$ = 0.1 mM). (*B*) The ratio of fluorescence intensity of the internal compartment vs. the "cytoplasm" decreases with time; similarly, the ratio of fluorescence intensity of the internal compartment vs the external medium decreases with time, indicating that the dinucleotide inside the internal compartment is slowly entering the cytoplasm.

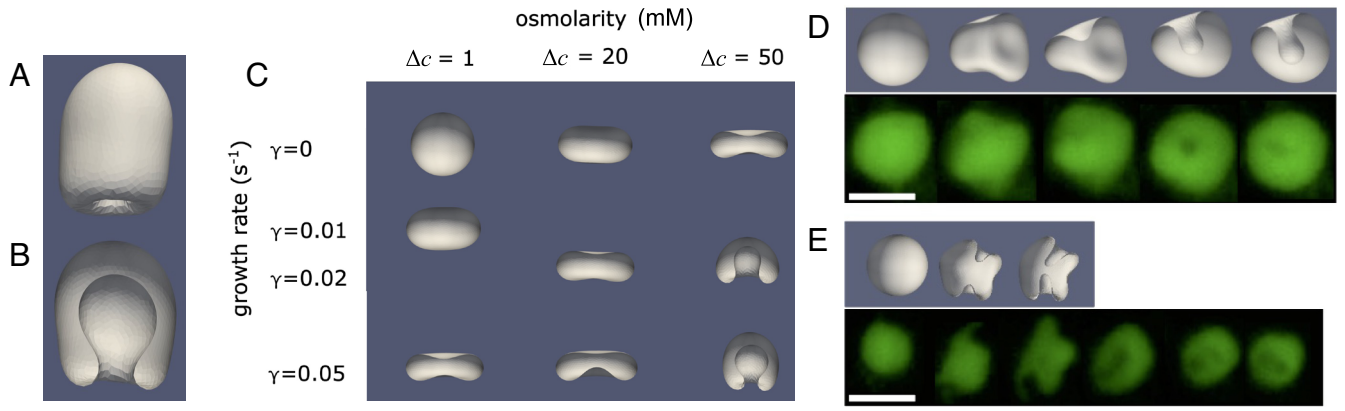

Fig. 5. Modeling of vesicle topological changes. For parameters used, see Table 2. (*A*) Side view and (*B*) cutaway of the final morphology of an initially spherical vesicle after 2 s of growth, with spontaneous formation of an incomplete inner bud, yet to be pinched off. (*C*) Final morphology of an initially spherical vesicle after 3 s of growth, for different values of the growth rate (γ) and osmolarity ($\Delta c = c_{out} - c_{in}$). Increasing the osmotic shock results in a higher effective growth rate, thereby reducing the threshold for vesiculation. (*D*) Comparison between simulations (gray) and experiments (green) showing inward vesiculation for a single compartment and (*E*) two compartments. Scale bars represent 5 μm. Further examples of inward vesiculation in simulations and experiments can be found in Movies S3–S11.

volume loss and area increase are consistent with those of prior work (24).

In terms of the morphological phase plane described in the study by Ruiz-Herrero et al. (19), the experimental parameter regime corresponds to invagination. We find that the added effect of osmotic pressures is parallel to a higher effective membrane growth rate and lowers the threshold for vesiculation (Fig. 5*C*). Our model recapitulates several of the behaviors observed experimentally, including the spontaneous onset of inward vesiculation on the correct timescale of seconds. In terms of the resulting vesicle morphology, we show that the resulting effect from a hyperosmotic shock corresponds to that of an increased effective membrane growth rate. This rationale is consistent with the progressively lower vesiculation threshold that is observed in experiments on vesicles subjected to increasing osmotic shocks (Fig. 2).

Furthermore, we find that reducing the magnitude of the spontaneous curvature and the bending modulus can lead to several internal invaginations forming (Fig. 5*E* and Movies S10 and S11). These results suggest that the addition of both micelles and an osmotic shock may contribute toward decreasing the bending modulus of the membrane. Indeed, this is consistent with our recent results showing that either a slight increase in pH or the addition of salt can decrease the bending modulus of fatty acid membranes (9).

In general, the time series of modeled geometries (Movies S9–S11) correspond well to experimental video microscopy data showing the endocytosis process (Movies S3–S8 and *Materials and Methods*). The changes in shape shown in the movies and in the sequences of images illustrated in Fig. 5 *D* and *E* take place on the timescale of seconds for both experiments and simulations. The relative timescales of water efflux, which is expected to be rapid, and micelle-driven surface area growth (*SI Appendix*), which is slower, indicate that water efflux and a modest increase in total area are adequate to drive endocytosis within seconds.

Several open questions remain. First, positive spontaneous curvature favors outward budding, whereas negative spontaneous curvature favors inward budding. This suggests that negative spontaneous curvature is important for passive endocytosis to occur, yet the mechanism of how negative spontaneous curvature would arise in our system remains unclear. One possibility is that the bilayer leaflets have an asymmetric interaction with water molecules or ions during simultaneous water efflux and membrane growth. Another hypothesis is that increased external salt bridges the carboxylate headgroups, either decreasing effective membrane area or perhaps changing effective lipid shape to favor negative curvature. Ultimately, while coarse-grained models are effective for predicting shape changes, molecular dynamics simulations of membrane packing might be necessary to reveal the underlying mechanism and cause (25). Second, although here we do explicitly solve for the hydrodynamics of the incompressible surrounding fluid, we have not studied the role of hydrodynamics in controlling the vesiculation behavior in detail. More specifically, systematically varying the membrane's spontaneous curvature and the bending modulus would be an interesting direction for future study.

Comparison to Passive Permeability. In light of our experimental demonstration of the release of both dinucleotides and HPTS from the endocytic compartment into the lumen, we also seek to further understand the utility of endocytosis as an inward-transport mechanism and estimate the time that is required for the vesicle's lumen to obtain various nutrients by passive diffusion across the compartment membrane. Such time scales can be estimated from the net flux (denoted by J, with units of number of molecules crossing unit area per unit time). The spontaneous transport of molecules along their concentration gradient across membranes is described by a simple equation

$$J = P_s \cdot \Delta C, \qquad [1]$$

where P_s is the permeability coefficient for the solute and $\Delta C (C_{in} - C_{out})$ is the concentration difference across the membrane. The number of molecules that cross a given area per unit time can be determined by rearranging Eq. **1** and the definition of flux

$$J = \frac{dN}{dt} \cdot \frac{1}{A}, \qquad [2]$$

into

$$dN = J \cdot dt \cdot A = P_s \cdot \Delta C \cdot dt \cdot A. \qquad [3]$$

Membrane permeability coefficients (P_s) for short oligomers up to the size of trinucleotides crossing oleic acid membranes have been previously measured (12). We consider trinucleotides, which can enhance nonenzymatic primer extension. The permeability of the oleic acid membrane to an average trinucleotide is $P_s \approx 0.21 \cdot 10^{-12}$

Table 1. Summary of different stimuli used to trigger shape changes in vesicles

Volume(Na-bicine); volume(micelles) (μL); *total number of vesicles analyzed*	Micelles (relative to the fatty acid concentration)			
Osmotic shock [Na-bicine] (mM)	1 equivalent (eqv.)	2 eqv.	5 eqv.	10 eqv.
25	2.7; 0.5; *4800*	2.7; 1; *4269*	2.7; 2.5; *3786*	2.7; 5; *695*
50	5.56; 0.5; *4395*	5.56; 1; *5897*	5.56; 2.5; *1730*	5.56; 5; *1576*
100	11.76; 0.5; *3840*	11.76; 1; *2941*	11.76; 2.5; *1697*	11.76; 5; *1169*

cm/s. In the presence of a 1 mM trinucleotide "pool", the number of trinucleotides that enter a GUV with a diameter of 4 μm from the external medium can be estimated from Eq. **3**, giving 0.06 trinucleotides per second. In other words, it takes approximately 16 s for a single trinucleotide to cross the oleic acid membranes when vesicles are surrounded by 1 mM trinucleotides.

We assessed the flux for a range of permeabilities (*SI Appendix*, Fig. S6) spanning values for common nutrients (10^{-10} and 10^{-13} cm/s). We found that it takes anywhere between 0.03 and 33 s for a single molecule to cross 4-μm-diameter oleic acid vesicles. It is clear that a protocell would have to reside within such a pool of nutrients for minutes to hours to acquire significant quantities of nutrients by passive diffusion.

This result is in stark contrast to passive endocytosis, which transports a parcel of nutrients inwards within seconds. In this scenario, a dramatic release event is not necessary for the nutrients to reach the putative cytoplasm. Instead, the molecules in the inner compartment can be slowly released into the main lumen of the protocell, where they can then interact with other components. For an inner compartment ¼ the diameter of a 4-μm-diameter GUV, 90% of molecules with permeability comparable to trinucleotides can be released into the lumen within 11 h (*SI Appendix*, Fig. S6*A*). This indicates that protocells that endocytose can absorb a substantial amount of nutrients from a pool despite interacting with it only briefly. Examples include a surface-immobilized protocell capturing nutrients from intermittently nutrient-rich streams of water, or a protocell capturing the released contents from a nearby burst protocell that would otherwise diffuse away.

This principle can be extended further to consider the transport of even larger oligomers. While permeabilities of longer oligomers through oleic acid membranes remain unknown, they are expected to have a lower permeability than trinucleotides. After approximately 4.7 h (*SI Appendix*, Fig. S6*B*), 10% of the molecules with a permeability of 10^{-13} cm/s are released from the interior compartment, with full release within 5 d. This result points to a remarkable function of passive endocytosis—a means of importing otherwise "membrane-impermeant" molecules.

Conclusions

We have shown that model primitive cell membranes are capable of invagination and inward vesiculation, leading to a complete topological transition to a vesicle-in-vesicle morphology. The number of internal compartments can be controlled by the rate of surface area growth, with increasingly strong osmotic shocks decreasing the rate of surface area growth necessary for vesiculation. We also recapitulated the main results and the relevant timescales in an out-of-equilibrium numerical model. We then found that such inward vesiculation events could lead to internalization of nutrient solutes including mononucleotides and oligonucleotides, drawing further parallels to endocytosis. Such processes could have helped primitive cells capture nutrients that are otherwise impermeable and could have also generated population diversity from a uniform starting solution of vesicles (Movie S12).

Materials and Methods

Materials. Oleic acid (C18:1) was purchased from NuChek Prep. DNA labeled with a fluorescent dye (5′-Cy5-$C_{(10)}$ $A_{(18)}$-3′) was synthesized by IDT. All other chemicals were purchased from Sigma-Aldrich and were used without any further purification. Data analysis was performed using ImageJ (version 1.53a), Python, and GraphPad Prism (version 8.4.0).

Preparation of Micelles and GUVs. One hundred millimolars of oleate micelles was prepared by dissolving 50 μmol neat oleic acid oil in 1 equivalent of NaOH solution to a volume of 500 μL with Millipore water (18.2 MΩ · cm). Fatty acid GUVs were made by resuspending the micelle solution in buffer stock (1 M Na-bicine, pH 8.45), sucrose stock, and Millipore water to the final concentration of 5 mM oleic acid, 50 mM Na-bicine buffer, and 200 mM sucrose as described previously (9). Encapsulation of fluorescent dyes was achieved by mixing the solute with the resuspension buffer before adding the micelles.

Vesicle Endocytosis. A 100 μL aliquot of the GUV suspension was carefully transferred to a 1.7 mL microcentrifuge tube (Fisher Scientific). These vesicles were subsequently diluted 1:9 into a buffer consisting of 50 mM Na-bicine at pH 8.45 and 200 mM glucose to a final oleic acid concentration of 0.5 mM, enabling good contrast of vesicles against the background when imaged under fluorescence microscopy. This diluted vesicle solution was then split into ten 100 μL aliquots. Vesicle endocytosis was initiated by adding micelles from a 100 mM stock solution and Na-bicine buffer from a 1 M stock solution to a 100 μL diluted aliquot, then mixing by inverting the tube for ∼5 s. The added volumes and concentrations corresponding to each condition are summarized and listed in Table 1. Vesicle suspensions were allowed to equilibrate for at least 1 h before microscopy.

Washing Endocytosed Vesicles. To dilute the free (unencapsulated) aqueous dye for imaging after passive endocytosis, the vesicle solution was diluted tenfold into a 200 mM glucose buffer that was identical in composition and pH to the original buffer, but lacked the lipids and dye. After centrifugation at 2,000 g for 30 s, the top 90% of volume was removed by pipetting. The remaining solution was then agitated to resuspend the vesicles.

Sequential Endocytosis Experiments. One hundred and fifty microliters of the washed vesicle suspension was transferred into one well of a Nunc Lab-Tek II 8-well chambered coverslip (Thermo Scientific) and the sample allowed to settle for 10 min to form a GUV monolayer at the bottom of the chamber. The endocytosis triggers were then pipetted into the open well in the sequence described in Fig. 3.

Specifically, the initial GUVs that encapsulated calcein blue (blue) were prepared following the protocol outlined in the "*Preparation of Micelles and GUVs*" section. After diluting the GUVs 1:9 into a buffer containing 50 mM Na-bicine at pH 8.45 and 200 mM glucose, to a final oleic acid concentration of 0.5 mM, the GUVs were allowed to settle for 10 min. Subsequently, the first endocytosis trigger was added to the well, resulting in a final concentration of 1 μM of 5′-Cy5-$C_{(10)}$ $A_{(18)}$-3′ along with ΔC_V = 100 mM Na-bicine and ΔC_A = 2.5 mM oleate. Inner compartments containing encapsulated 5′-Cy5-$C_{(10)}$ $A_{(18)}$-3′ (magenta) derived from the external solution were formed (see also Movie S1). After 1 h, a second round of passive endocytosis was initiated by pipetting in a second stimulus to a final concentration of 5 μM Fluorescein-12-UTP, ΔC_V = 100 mM Na-bicine and ΔC_A = 2.5 mM oleate. The changes in Na-bicine and oleate concentration were relative to the end of the first endocytic event; the final Na-bicine concentration was 250 mM and the final oleate concentration was 5.5 mM. This second trigger led to the formation of new inner compartments containing encapsulated Fluorescein-12-UTP (yellow) derived from the external solution.

Table 2. Parameters used in simulations of growing permeable vesicles under osmotic shock

				Values used for figures and movies					
	Symbol	Units	Range tested	5 *A* and *B*	5*D*	5*E*	S9	S10	S11
Initial diameter	R	μm	1						
Water permeability	P_f	cm/s	14e-3						
Growth rate	γ	s^{-1}	0 to 2.5	0.02	2.5	0.75	0.1	0.02	0.007
Viscosity	μ	dyn/cm×s	0.01						
Density	ρ	g/cm^3	1						
Osmolarity	Δc	mM	10 to 100	50	10	100	10	50	50
Specific volume	v_w	cm^3/mol	20						
Spontaneous curvature	c_0	μm	−0.2 to −1	−1	−0.66	−0.2	−1	−0.66	−0.4
Bending modulus	K_b	k_BT	2 to 100	10	100	10	10	3	2
Total time	T	s	1 to 3						

Confocal Microscopy. Confocal images were collected using a Nikon A1R HD25 confocal laser scanning microscope equipped with LU-N4/N4S 4-laser unit.

Vesicle Endocytosis Movies S3–S8**.** An aliquot of the GUV suspension encapsulating 1 mM HPTS was diluted 1:9 into a buffer consisting of 50 mM Na-bicine, pH 8.45, and 200 mM glucose to a final oleic acid concentration of 0.5 mM. One hundred and fifty microliters of the diluted suspension was transferred into one well of a Nunc Lab-Tek II 8-well chambered coverslip (Thermo Scientific) and the sample allowed to settle for 10 min to form a GUV monolayer at the bottom of the chamber. Two microliters of a solution containing both 500 mM Na-bicine and 25 mM oleate micelles was then pipetted into the well containing the diluted GUVs. Epifluorescence microscopy was performed using a Nikon TE2000-U inverted microscope. A blue LED was used to excite the sample using a CoolLED pE-300^{ultra} system, and images were captured using a pco.edge 4.2 sCMOS camera.

Immersed Boundary Method Simulations. To simulate growing, permeable vesicles under osmotic shock, we used the immersed boundary method to simulate the coupled fluid–structure interaction of permeable vesicles growing in an incompressible aqueous solution (26). Given the complexity of possible changes in vesicle morphology, it was important to perform simulations in three dimensions, and for computational efficiency, we used the method described in the study by Fai et al. (27).

For simplicity, we held the inner and outer osmolyte concentrations constant and did not account for solute exchange across the membrane (i.e., we set $P_s = 0$ in the notation of Sacerdote et al.) (24). Given that the rate of solute exchange is typically much lower than that of solvent, this approximation is expected to be reasonable for the relatively short timescales of interest here. Further details can be found in *SI Appendix*, Appendix I.

Data, Materials, and Software Availability. All study data are included in the article, *SI Appendix* and/or the OSF repository (https://osf.io/r4zsp/?view_only=6da09fcb508d4ab2b93c1d13ee406b18) (28).

ACKNOWLEDGMENTS. Y.K. acknowledges the support from the Human Frontier of Science Program (RGP0032/2022 to Y.K.), DP1GM149751, 1R01NS112139-01A1, and Ono Pharma Foundation. T.G.F. acknowledges the support from NSF MCB-2213583 and DMS-1913093. J.W.S. is an investigator of the Howard Hughes Medical Institute. This work was funded in part by a grant from the Simons Foundation (290363) to J.W.S. A.W. acknowledges support from the Australian Research Council (DE210100291) and the Human Frontier Science Program (RGP0029/2020 to A.W.).

Author affiliations: [a]Department of Chemistry and Chemical Biology, Harvard University, Cambridge, MA 02138; [b]Department of Molecular Biology, Center for Computational and Integrative Biology, Massachusetts General Hospital, Boston, MA 02114; [c]School of Chemistry, University of New South Wales Sydney, Bedegal Country, Sydney, NSW 2052, Australia; [d]Australian Centre for Astrobiology, University of New South Wales Sydney, Bedegal Country, Sydney, NSW 2052, Australia; [e]ARC Centre of Excellence in Synthetic Biology, University of New South Wales Sydney, Bedegal Country, Sydney, NSW 2052, Australia; [f]Neuroscience Institute, University of Chicago, Chicago, IL 60637; [g]Department of Chemistry, University of Chicago, Chicago, IL 60637; [h]Institute of Biophysical Dynamics, University of Chicago, Chicago, IL 60637; [i]Department of Mathematics, Brandeis University, Waltham, MA 02453; and [j]HHMI, Massachusetts General Hospital, Boston, MA 02114

1. J. P. Schrum, T. F. Zhu, J. W. Szostak, The origins of cellular life. *Cold Spring Harb. Perspect. Biol.* **2**, a002212 (2010).
2. R. V. Sole, Evolution and self-assembly of protocells. *Int. J. Biochem. Cell B* **41**, 274–284 (2009).
3. A. J. Dzieciol, S. Mann, Designs for life: Protocell models in the laboratory. *Chem. Soc. Rev.* **41**, 79–85 (2012).
4. D. W. Deamer, R. M. Pashley, Amphiphilic components of the Murchison carbonaceous chondrite: Surface properties and membrane formation. *Orig. Life Evol. Biosph.* **19**, 21–38 (1989).
5. D. W. Deamer, G. L. Barchfeld, Encapsulation of macromolecules by lipid vesicles under simulated prebiotic conditions. *J. Mol. Evol.* **18**, 203–206 (1982).
6. S. S. Mansy, Model protocells from single-chain lipids. *Int. J. Mol. Sci.* **10**, 835–843 (2009).
7. A. Wang, J. W. Szostak, Lipid constituents of model protocell membranes. *Emerg. Top Life Sci.* **3**, 537–542 (2019).
8. T. F. Zhu, J. W. Szostak, Coupled growth and division of model protocell membranes. *J. Am. Chem. Soc.* **131**, 5705–5713 (2009).
9. J. T. Kindt, J. W. Szostak, A. Wang, Bulk self-assembly of giant, unilamellar vesicles. *ACS Nano* **14**, 14627–14634 (2020).
10. E. Blöchliger, M. Blocher, P. Walde, P. L. Luisi, Matrix effect in the size distribution of fatty acid vesicles. *J. Phys. Chem. B* **102**, 10383–10390 (1998).
11. K. Adamala, J. W. Szostak, Nonenzymatic template-directed RNA synthesis inside model protocells. *Science* **342**, 1098–1100 (2013).
12. D. K. O'Flaherty *et al.*, Copying of mixed-sequence RNA templates inside model protocells. *J. Am. Chem. Soc.* **140**, 5171–5178 (2018).
13. P. G. Barton, F. D. Gunstone, Hydrocarbon chain packing and molecular-motion in phospholipid bilayers formed from unsaturated lecithins. Synthesis and properties of 16 positional isomers of 1,2-dioctadecenoyl-sn-glycero-3-phosphorylcholine. *J. Biol. Chem.* **250**, 4470–4476 (1975).
14. M. C. Blok, E. C. M. Vanderneutkok, L. L. M. Vandeenen, J. Degier, Effect of chain-length and lipid phase-transitions on selective permeability properties of liposomes. *Biochim. Biophys. Acta* **406**, 187–196 (1975).
15. S. S. Mansy, Membrane transport in primitive cells. *Cold Spring Harb. Perspect. Biol.* **2**, a002188 (2010).
16. W. Zong *et al.*, A fissionable artificial eukaryote-like cell model. *J. Am. Chem. Soc.* **139**, 9955–9960 (2017).
17. R. Lipowsky, The conformation of membranes. *Nature* **349**, 475–481 (1991).
18. P. Peterlin, V. Arrigler, K. Kogej, S. Svetina, P. Walde, Growth and shape transformations of giant phospholipid vesicles upon interaction with an aqueous oleic acid suspension. *Chem. Phys. Lipids* **159**, 67–76 (2009).
19. T. Ruiz-Herrero, T. G. Fai, L. Mahadevan, Dynamics of growth and form in prebiotic vesicles. *Phys. Rev. Lett.* **123**, 038102 (2019).
20. R. J. Bruckner, S. S. Mansy, A. Ricardo, L. Mahadevan, J. W. Szostak, Flip-flop-induced relaxation of bending energy: Implications for membrane remodeling. *Biophys. J.* **97**, 3113–3122 (2009).
21. A. Saminathan *et al.*, A DNA-based voltmeter for organelles. *Nat. Nanotechnol.* **16**, 96–103 (2021).
22. R. Lipowsky, Remodeling of membrane compartments: Some consequences of membrane fluidity. *Biol. Chem.* **395**, 253–274 (2014).
23. S. M. Fujikawa, I. A. Chen, J. W. Szostak, Shrink-wrap vesicles. *Langmuir* **21**, 12124–12129 (2005).

24. M. G. Sacerdote, J. W. Szostak, Semipermeable lipid bilayers exhibit diastereoselectivity favoring ribose. *Proc. Natl. Acad. Sci. U.S.A.* **102**, 6004–6008 (2005).
25. A. J. Markvoort *et al.*, Vesicle deformation by draining: Geometrical and topological shape changes. *J. Phys. Chem. B* **113**, 8731–8737 (2009).
26. C. H. Wu, T. G. Fai, P. J. Atzberger, C. S. Peskin, Simulation of osmotic swelling by the stochastic immersed boundary method. *Siam. J. Sci. Comput.* **37**, 660–688 (2015).
27. T. G. Fai, B. E. Griffith, Y. Mori, C. S. Peskin, Immersed boundary method for variable viscosity and variable density problems using fast constant-coefficient linear solvers I: Numerical method and results. *Siam. J. Sci. Comput.* **35**, 1132–1161 (2013).
28. S. J. Zhang, A. Wang, Passive endocytosis in model protocells. Open Science Framework. https://osf.io/r4zsp/?view_only=6da09fcb508d4ab2b93c1d13ee406b18. Deposited 23 May 2023.

Supplementary Information for
Passive endocytosis in model protocells

Stephanie J. Zhang[1,2], Lauren A. Lowe[3,4,5], Palapuravan Anees[6,7], Yamuna Krishnan[6,7,8], Thomas G. Fai[9]*, Jack W. Szostak[1,2,7,10]*, and Anna Wang[3,4,5]*

[1] Department of Chemistry and Chemical Biology, Harvard University, 12 Oxford Street, Cambridge, Massachusetts 02138, United States;
[2] Department of Molecular Biology, Center for Computational and Integrative Biology, Massachusetts General Hospital, Boston, MA 02114, United States;
[3] School of Chemistry, UNSW Sydney, Bedegal Country, New South Wales 2052, Australia
[4] Australian Centre for Astrobiology, UNSW Sydney, Bedegal Country, New South Wales 2052, Australia
[5] ARC Centre of Excellence in Synthetic Biology, UNSW Sydney, Bedegal Country, New South Wales 2052, Australia
[6] Neuroscience Institute, University of Chicago, Chicago, IL 60637, United States;
[7] Department of Chemistry, University of Chicago, Chicago, IL 60637, United States;
[8] Institute of Biophysical Dynamics, University of Chicago, Chicago, IL 60637, United States;
[9] Department of Mathematics, Brandeis University, Waltham, Massachusetts 02453, United States;
[10] Howard Hughes Medical Institute, Massachusetts General Hospital, Boston, MA 02114, United States;

*co-corresponding authors: Thomas G. Fai, Jack W. Szostak, and Anna Wang

Email: tfai@brandeis.edu**,** jwszostak@uchicago.edu, or anna.wang@unsw.edu.au

Present address: Stephanie J. Zhang, Department of Pathology, Brigham and Women's Hospital, Harvard Medical School, 60 Fenwood Rd, Boston, Massachusetts 02115, USA.

This PDF file includes:

Calculations for surface area increase

Here we seek to estimate an upper bound for change in surface area that occurs during a topological change, which usually completes within seconds (see Movie S1, Movies S3-S8). The presumed growth process is that described by Chen and coworkers: an initial fast micelle growth phase leads to a 40% increase in surface area within 50 seconds, with further growth occurring via a different mechanism over minutes.[1]

To estimate the increase in surface area from the addition of micelles, we analyze the vesicle sizes before and after micelle addition. Figure 2 shows that the addition of 10 equivalents of micelles and a 25 mM osmotic shock results in ~15% of vesicles having at least 3 compartments. For such a case, assuming the compartment radius (r) is half that of the external membrane (radius R), the final volume of the lumen is $\frac{4}{3}\pi\mathrm{R}^3 - 3\frac{4}{3}\pi\mathrm{r}^3 = \frac{4}{3}\pi\mathrm{R}^3 - 4\pi(\frac{\mathrm{R}}{2})^3 = \frac{5}{6}\pi\mathrm{R}^3$. The lumen volume should have decreased by a factor of 2/3 following the osmotic shock, thus the original volume of the vesicle prior to the osmotic shock and micelle addition is $\frac{15}{12}\pi\mathrm{R}^3$. Because the starting vesicle was a sphere, the initial radius is given by $(\frac{\frac{15}{12}\pi\mathrm{R}^3}{\frac{4}{3}\pi})^{1/3} \sim 0.979\ \mathrm{R}$. The initial surface area is thus $4\pi\mathrm{R}^2 \cdot 0.979^2$. Comparing this to a final surface area of $4\pi\mathrm{R}^2 + 4\pi(\frac{\mathrm{R}}{2})^2 \cdot 3 = 7\pi\mathrm{R}^2$ reveals a surface area increase of 1.8-fold. This is in agreement with the results from Zhu *et al.*, which found a doubling in surface area over five minutes upon the addition of 5 equivalents of micelles to multilamellar vesicles.[2] The increase in surface area over the timescales of the endocytic event are therefore expected to be no more than two-fold.

1. Chen, I. A. & Szostak, J. W. A Kinetic Study of the Growth of Fatty Acid Vesicles. *Biophys J* **87**, 988–998 (2004).

2. Zhu, T. F. & Szostak, J. W. Coupled Growth and Division of Model Protocell Membranes. *Journal of the American Chemical Society* **131**, 5705–5713 (2009).

Figure S1. Two-dimensional schematic of topological transformations from a GUV into a stomatocyte shape (a), or a vesicle-in-vesicle structure (b).

Figure S2. Whether an internal bud is connected to or disconnected from the outside can be distinguished by the addition of an impermeable aqueous dye. Schematics showing the outcomes of adding such a dye are shown in (a) and (b). (c) Confocal micrographs of vesicles containing calcein blue (blue) and endocytic compartments, after the addition of aqueous dye Alexa 594 hydrazide (red). The separate channels and merged image confirm that the internal compartments are disconnected from the outside. Scale bars represent 5 μm.

Experimental conditions: A GUV solution consisting of 5 mM of oleic acid encapsulating 1 mM calcein blue were prepared as described in the Materials and Methods section. The resulting solution was diluted 1:9 in a buffer composed of 50 mM Na-bicine (pH 8.45) and 200 mM glucose to obtain a final oleic acid concentration of 0.5 mM. Micelles from a 100 mM stock solution and Na-bicine buffer from a 1 M stock solution were added to 100 μL of the diluted vesicle solution, where ΔC_V = 100 mM Na-bicine and ΔC_A = 1 mM oleate. After allowing the vesicle suspensions to equilibrate for at least 1 hour, Alexa 594 hydrazide was introduced to a final concentration of 10 μM. The suspensions were mixed by inverting the tube for approximately 5 seconds before microscopy.

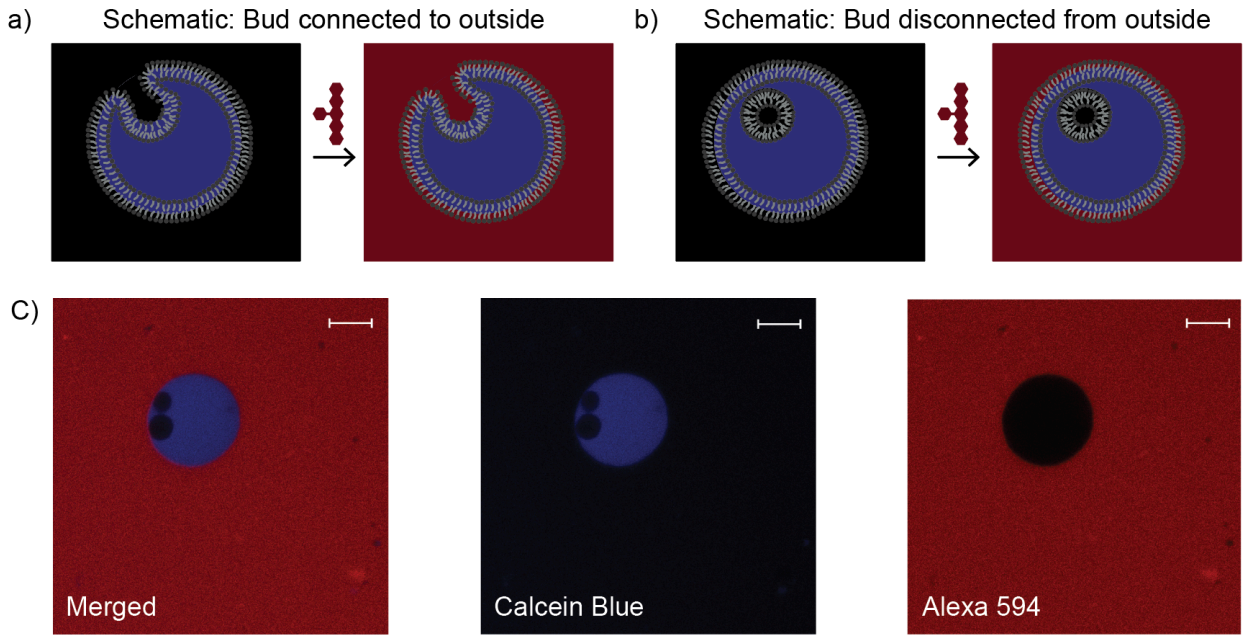

Figure S3. Whether an internal bud is connected to or disconnected from the external membrane can be distinguished by the addition of an impermeable membrane dye. Schematics showing the consequence of adding the membrane dye Voltair^{PM} (yellow) to the vesicles are shown in (a) and (b). (c) Confocal micrographs of vesicles containing calcein blue (teal) and endocytic compartments, after the addition of the membrane dye Voltair^{PM} (yellow). The separate channels and merged image confirm that the internal compartments are disconnected from the outside. Scale bars represent 5 μm.

Experimental conditions: A GUV solution consisting of 5 mM of oleic acid encapsulating 1 mM calcein blue were prepared as described in the Materials and Methods section and subsequently diluted 1:9 into a buffer containing 50 mM Na-bicine (pH 8.45) and 200 mM glucose, resulting in a final oleic acid concentration of 0.5 mM. Micelles from a 100 mM stock solution and Na-bicine buffer from a 1 M stock solution were added to the diluted vesicle solution, causing a change in concentration denoted as ΔC_V = 100 mM Na-bicine and ΔC_A = 1 mM oleate. Following at least 1 hour of equilibration, Voltair^{PM} was introduced to a final concentration of 250 nM. The suspensions were mixed by inverting the tube for approximately 5 seconds before microscopy.

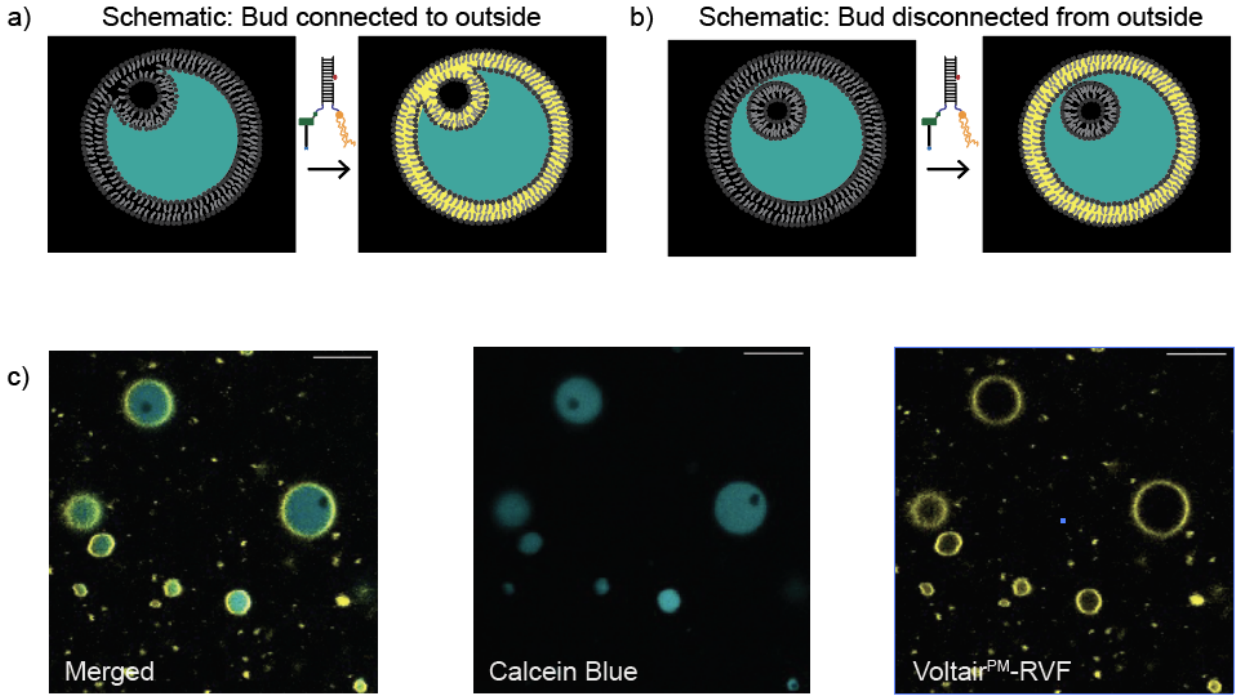

Figure S4. To calculate the average time T_1 required for a single molecule to enter a 4-μm-diameter vesicle, Equation (3) is rearranged and dN is set to 1, giving $T_1 = 1/\left(P_s \cdot \Delta C \cdot A\right)$. This is calculated for a range of permeabilities spanning values for common nutrients (P_s ranging from 10^{-10} to 10^{-13} cm/s), and a ΔC = 1 mM nutrient pool.

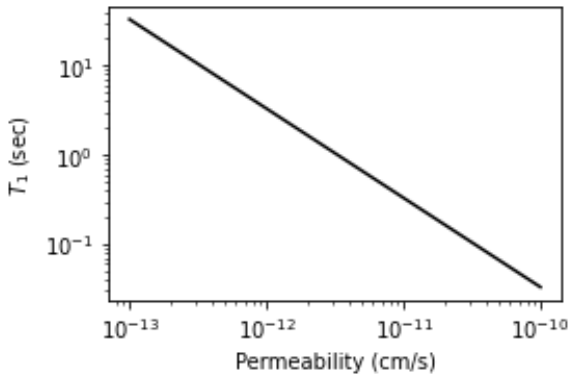

Figure S5. Internal compartments can slowly deliver nutrients of low permeability to the main lumen or 'cytoplasm' of a protocell. (a) 1 mM of HPTS, a relatively impermeable substrate, is encapsulated in the interior compartment via one hyperosmotic shock coupled with micelle addition (ΔC_V = 100 mM Na-bicine, ΔC_A = 2.5 mM oleate). (b) The ratio of fluorescence intensity of the internal compartment vs the 'cytoplasm' decreases with time; similarly, the ratio of fluorescence intensity of the internal compartment vs the external medium decreases with time, indicating that the HPTS inside the internal compartment is slowly entering the 'cytoplasm'.

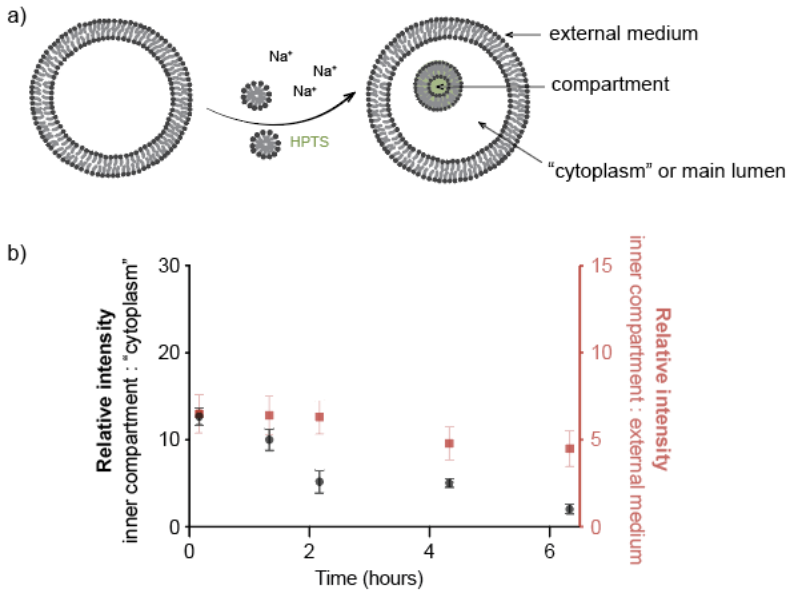

Figure S6. The release and retention of molecules with permeabilities of 10^{-12} and 10^{-13} cm/s across the membranes as a function of time is calculated by integrating Equation (3). (a) The intersection of the black dashed line (y = 0.9) and the black solid line indicates that 90% of the molecules with P_s = 10^{-12} cm/s will enter the main lumen of the protocell from the compartment within 11 hours. (b) The intersection of the black dashed line (y = 0.1) and the black solid line indicates that 10% of the molecules with P_s = 10^{-13} cm/s will enter the main lumen of the protocell from the compartment within 5 hours.

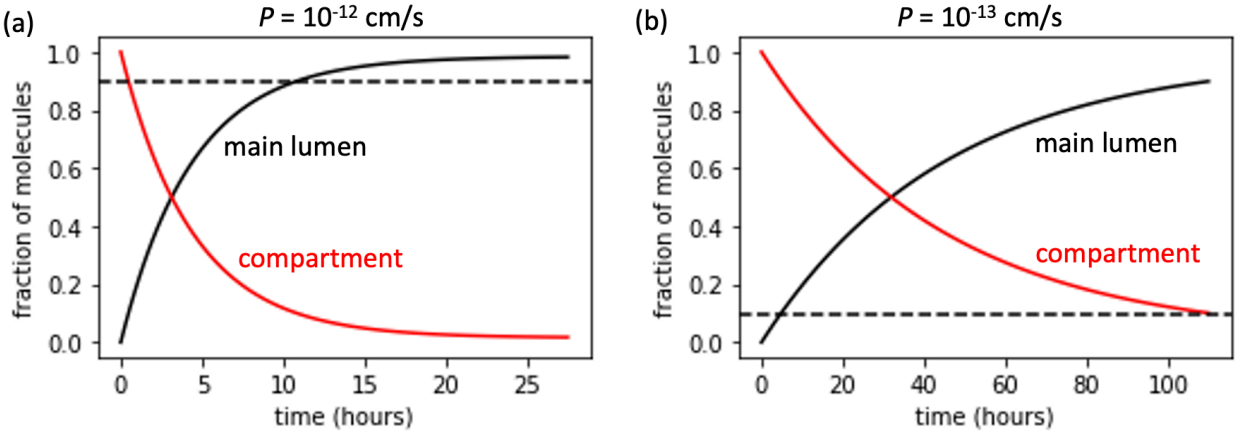

Movie S1. This real-time movie shows the topological transformation (prolate–oblate–stomatocyte-sphere) upon an osmotic shock and micelle addition (stimulus A; ΔC_V = 100 mM, ΔC_A = 1 mM). Prolate spheroid vesicles appeared to keep their shape for ~1 s, and then transformed into an oblate spheroid then stomatocyte within the next ~2 s. Subsequently, stomatocytes transformed into sphere-in-sphere structures via further invagination and pinching off of the internal vesicles. Each micrograph is 126 μm by 126 μm.

Movie S2. 3D reconstruction of vesicle-in-vesicle structures from sectional image slices along the *z*-axis, from slices taken using confocal microscopy.

Movies S3-S8. These real-time movies show the transformation (prolate–oblate–stomatocyte-sphere) upon an osmotic shock and micelle addition delivered by pipetting a small aliquot of concentrated micelles and buffer in the vicinity of the vesicles (see Methods). Depending on the proximity of the pipetted stimulus, the vesicles formed either one or more internal compartments. Each micrograph is 111 μm by 111 μm unless otherwise indicated.

Movies S9-S11. These movies show the simulated transformation (prolate–oblate–stomatocyte) upon an osmotic shock and micelle addition. Depending on the values of parameters used (see Table 2), in particular the bending modulus K_b and the spontaneous curvature c_0, the vesicles formed either one or more internal compartments.

Movie S12. This movie shows that population diversity can be achieved from a uniform starting solution of vesicles, because of multiple heterogeneous stimuli (conditions as per Figure 3).

APPENDIX I

IMMERSED BOUNDARY SIMULATIONS

A. Formulation

In order to simulate the dynamics of growing fatty acid vesicles immersed in fluid, we use the immersed boundary method previously described in [1]. This method allows us to compute the emergent deformations of the vesicle as a function of the growth rate. We highlight the key aspects of this method here for the readers' convenience, following closely the description in [1].

The vesicle is modeled as an elastic shell having bending rigidity B, spontaneous curvature c_0, and local stretching resistance k_a, and the fluid surrounding the vesicle is modeled explicitly by the incompressible Navier-Stokes equations with fluid velocity $\mathbf{u}$ and pressure p. The fluid-structure interaction is specified with the vesicle parameterized in Lagrangian coordinates $\mathbf{q} = (q,r)$ and the vesicle configuration $\mathbf{X}(\mathbf{q},t)$ in cartesian coordinates. At any instant in time t, the vesicle configuration $\mathbf{X}(\mathbf{q},t)$ determines the elastic force density $\mathbf{F}(\mathbf{q},t)$ exerted on the fluid. In addition, the elastic material moves at a velocity

$$\frac{\partial \mathbf{X}}{\partial t}(\mathbf{q},t) = \mathbf{U}(\mathbf{q},t) + K\left(\Delta\phi + \frac{(\mathbf{F}(\mathbf{q},t)\cdot\mathbf{N}(\mathbf{q},t))}{\left\|\frac{\partial \mathbf{X}}{\partial r}\times\frac{\partial \mathbf{X}}{\partial s}\right\|}\right)\mathbf{N}(\mathbf{q},t), \tag{S.1}$$

where $\mathbf{U}(\mathbf{q},t) = \mathbf{u}(\mathbf{X}(\mathbf{q},t),t)$ is the fluid velocity at the vesicle membrane, $\mathbf{N}$ is the unit surface normal, $\Delta\varphi = (c_{in} - c_{out})k_BT$ is the osmotic pressure drop, and K is the vesicle permeability. The velocity above is similar to those used previously for porous membranes [2–4], here with an additional osmotic pressure term. It is equivalent to specifying the local flux across the membrane to be proportional to the pressure jump [5].

Vesicle growth is realized through increasing the vesicle surface area over time uniformly over the surface. In particular, the vesicle is assumed to incorporate additional lipid amphiphiles at a constant rate γ per unit area, so that $\mathrm{d}A/\mathrm{d}t = \gamma A$. On the other hand, changes in volume are determined implicitly through (S.1). In the limit of an impermeable membrane with $K = 0$, the vesicle moves at the local velocity of the incompressible fluid so that the enclosed volume is

conserved. For nonzero $K > 0$, however, the membrane porosity causes the enclosed volume to change over time. In particular, in the absence of membrane forces ($\mathbf{F} \equiv 0$), we have:

$$\mathrm{d}V/\mathrm{d}t = KA\Delta\varphi, \tag{S.2}$$

so that osmotic shocks lead to vesicle swelling or shrinking. However, since the vesicle is assumed to be elastic, we have $\mathbf{F} \neq 0$ in general, and the changes in volume are the result of both osmotic pressures and elastic stresses on the membrane.

Remeshing is done periodically to keep the triangles in the mesh as regular as possible through growth and deformation, following the remeshing operations described in [6]. To avoid dealing with the changing topologies (which is nontrivial from both the modeling and numerical perspectives), simulations are halted prior to any budding or vesiculation events.

---

[1] T. Ruiz-Herrero, T. G. Fai, and L. Mahadevan, "Dynamics of growth and form in prebiotic vesicles," Phys. Rev. Lett., vol. 123, no. 3, p. 038102, 2019.

[2] Y. Kim and C. S. Peskin, "2–D parachute simulation by the immersed boundary method," SIAM J. Sci. Comput., vol. 28, pp. 2294–2312, 2006.

[3] Y. Kim, Y. Seol, M.-C. Lai, and C. S. Peskin, "The immersed boundary method for two-dimensional foam with topological changes," Comm. Comput. Phys., vol. 12, no. 2, p. 479, 2012.

[4] Y. Kim, M.-C. Lai, C. S. Peskin, and Y. Seol, "Numerical simulations of three-dimensional foam by the immersed boundary method," J. Comput. Phys., vol. 269, pp. 1–21, jul 2014.

[5] Z. Li and M.-C. Lai, "The immersed interface method for the Navier–Stokes equations with singular forces," J. Comput. Phys., vol. 171, pp. 822–842, 2001.

[6] M. Botsch, L. Kobbelt, M. Pauly, P. Alliez, B. Levy, L. Kobbelt, M. Pauly, P. Alliez, and B. Levy, Polygon Mesh Processing. A K Peters/CRC Press, 2010.